ICNMM2008-62199

SLIP-FLOW PRESSURE DROP IN MICROCHANNELS OF GENERAL CROSS-SECTION

A. Tamayol
Department of Mechanical Engineering,
University of Victoria, BC, Canada
atamayol@uvic.ca

M. Bahrami
Mechatronic Systems Engineering,
School of Engineering Science,
Simon Fraser University, BC, Canada
mbahrami@sfu.ca

P. Taheri
Department of Mechanical Engineering,
University of Victoria, BC, Canada
peymant@uvic.ca

ABSTRACT

In the present study, a compact analytical model is developed to determine the pressure drop of fully-developed, incompressible, and constant properties slip-flow through arbitrary cross-section microchannels. An averaged first-order Maxwell slip boundary condition is considered. Introducing a relative velocity, the difference between the bulk flow and the boundary velocities, the axial momentum reduces to the Poisson's equation with homogeneous boundary condition. Square root of area is selected as the characteristic length scale. Bahrami et al.'s model, which was developed no-slip boundary condition, is extended to cover the slip-flow regime in this study. The proposed model is a function of geometrical parameters of the channel: cross-sectional area, perimeter, polar moment of inertia and the Knudsen number. The model is successfully validated against existing numerical and experimental data from different sources in the literature for several shapes, including: circular, rectangular, trapezoidal, and double-trapezoidal cross-sections and a variety of gases such as: nitrogen, argon, and helium.

NOMENCLATURE

A	Cross-sectional area, m^2
D_h	Hydraulic diameter, m
$E(.)$	Complete elliptic integral of the second kind
fRe	Poiseuille number
I_p	Polar moment of inertia, m^4
I_p^*	Dimensionless polar moment of inertia, I_p/A^2
Kn	Knudsen number
$\mathcal{L}$	Characteristics length, m
P	Pressure, N/m^2
Re	Reynolds number
$\sqrt{A}$	Square root of area, m
u	Axial velocity, m/s
u_s	Local slip-velocity, m/s
$\bar{u}_s$	Average slip-velocity, m/s
U	Relative velocity, m/s

Greek symbols

Γ	Perimeter, m
ε	Aspect ratio
λ	Molecular mean free path, m
μ	Viscosity, $N.S/m^2$
σ	Tangential momentum accommodation factor
$\bar{\tau}_w$	Averaged wall shear stress, N/m^2
τ_w	Local shear stress, N/m^2
Φ	reduction of friction coefficient in slip condition, $fRe_{\sqrt{A}}\big/fRe_{\sqrt{A}}^{no-slip}$

1 INTRODUCTION

The fast-paced growth of microfluidic systems and their applications in electronics cooling, aerospace, MEMS, medical and biomedical devices has motivated many researchers to investigate microscale transport phenomena [1-3]. Microchannels are essential components of many microfluidic devices [4]. Several factors that differentiate microscale from conventional flows have been identified through a number of experimental, numerical, and analytical studies. These include: non-continuum regimes, surface roughness, and compressibility effects [5-7]. Due to the small size of these channels, the length scale is comparable to molecular mean free path; thus, deviation from the continuum theory should be considered. The non-dimensional parameter

used for analyzing this deviation is the Knudsen number, defined as:

$$Kn = \frac{\lambda}{\mathcal{L}} \qquad (1)$$

where, λ is the molecular mean free path and $\mathcal{L}$ is an appropriate length scale of the channel. When the Knudsen number is in the range of $0.001 < Kn < 0.1$ a non-equilibrium state occurs very close to the wall, which is initiated from domination of molecular collisions with the walls over intermolecular collisions [8]. Hence, no-slip boundary condition is no longer valid on channels boundaries, where a slip-velocity exists. However, for the rest of the flow, the continuum assumption still holds. This is called *slip-flow regime*.

Pressure drop in micro conduits with different cross-sections including non-continuum effects has been the subject of several investigations. In rarefied gas flow, the friction factor reduces as the Knudsen number increases. This is demonstrated theoretically by Pfahler et al. [9], Ebert and Sparrow [10], Harley et al. [11], Morini and Spiga [12], and Beskok and Karniadakis [13]. Experimental studies conducted by Harley et al. [11], Choi et al. [14], You et al. [15], Arkilic et al. [16, 17], Araki et al. [18], and Kim et al.[4] confirm that the continuum assumption with no-slip velocity on walls is unable to predict the flow behaviour in microchannels in this range of Knudsen number.

Pfahler et al. [9] performed one of the first analytical and experimental investigations on rarefied flows. They reported the existence of slip-flow in microchannels through measuring an increase in mass flow rate, when compared with the predicted values from the continuum (no-slip) theory.

Kim et al. [4] reported experimental data for rarefied flow through microtubes over the range of $0.0008 < Kn < 0.09$ and $0.03 < Re < 30$. They tested several gases such as: nitrogen, helium, and argon. Araki et al. [18] reported results for pressure drop in trapezoidal and triangular channels in slip-flow regime where $0.011 < Kn < 0.035$ and $0.05 < Re < 4.2$ range. Arkilic et al. [16] included compressibility effects in their tests by conducting experiments in relatively higher Mach numbers. They also proposed an analytical model for analyzing compressible slip-flow in trapezoidal silicon microchannels; they did not report the range of Mach number in their tests. Arkilic et al. [17] conducted experiments to determine the effects of tangential momentum accommodation on the mass flow rate through trapezoidal microchannels, in the slip-flow regime.

Ebert and Sparrow [9] formulated an analytical solution for slip-flow through rectangular channels. They realized that the effect of slip is to flatten the velocity distribution relative to that of a continuum flow. Assuming first order slip boundary condition, Morini and his coworkers [12, 19] performed numerical studies for determination of pressure drop through microchannels of rectangular, circular, trapezoidal, and double trapezoidal cross-sections and reported their results in a tabular form for a range of cross-section aspect ratio for the slip-flow regime. Using similar boundary conditions Khan and Yovanovich [20] developed a solution for fluid flow and convective heat transfer in rectangular microchannels in slip-flow regime. Duan and Muzychka [21] proposed a model for the pressure drop of slip-flow through non-circular microchannels using the solution of the rectangular duct. They compared their model

with the numerical data of Morini et al. [19] for common geometries. Their model is a function of the cross-section aspect ratio defined for each geometry.

As a result of recent advances in micro fabrication techniques, microchannels with different cross-sectional geometries are fabricated for both commercial and scientific purposes. Bahrami et al. [22, 23] developed a general model for prediction of pressure drop in microchannels of arbitrary cross-section. Using the analytical solution of elliptical duct and the concept of Saint-Venant principal in torsion, they showed that the Poiseuille number is a function of the polar moment of inertia, area and perimeter of the cross-section of the channel. Their model showed good agreement with experimental and numerical data for a wide variety of cross-sections such as: rectangular, trapezoidal, triangular, circular, and moon shaped. Bahrami et al.'s model; however, is restricted to no-slip velocity regime. Their model; however, is restricted to no-slip velocity regime. The objective of this paper is to extend Bahrami et al.'s [22, 23] model to the slip-flow regime.

In this study, a general model is developed for predicting the Poiseuille number of fully-developed flow in arbitrary cross-section microchannels with slip regime. The proposed model is validated with numerical and experimental data from different sources for a variety of geometries, including: circular, rectangular, trapezoidal, and double-trapezoidal cross-sections and several gases such as: nitrogen, argon, and helium.

2 PROBLEM STATEMENT

Fully-developed laminar, constant properties, and incompressible flow in microchannels of constant general cross-section is considered (Fig. 1). Based on the Knudsen number, flows regimes can be categorized into four groups: continuum (no-slip), slip-flow, transition, and molecular flows [24]. For slip-flow regime where $0.001 < Kn < 0.1$ errors due to the use of Navier- Stoke's (NS) equations are negligible. However, no-slip boundary condition is no longer valid on walls and a slip-velocity should be considered [8]. The first-order Maxwell boundary condition for slip-velocity is:

$$u_s = \frac{\sigma - 2}{\sigma} \lambda \frac{\partial u}{\partial n}\Big|_{wall} \qquad (2)$$

where the thermal creep effects on the solid-fluid interface is neglected [24]. Here, u_s is the local slip-velocity, σ is tangential momentum accommodation factor which is considered unity for most of engineering applications [25], λ is the molecular mean free path, and *n* is the normal vector to the wall.
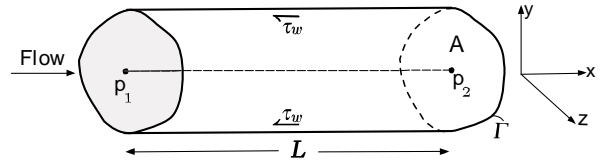

FIGURE 1.FLOW IN ARBITRARY CROSS-SECTION MICROCHANNEL

Using abovementioned assumptions, the momentum equation reduces to:

$$\frac{dP}{dx} = \mu \left(\frac{\partial^2 u}{\partial y^2} + \frac{\partial^2 u}{\partial z^2} \right) \qquad (3)$$

This equation should be solved along with the following boundary condition:

$$u_s = \frac{\sigma - 2}{\sigma} \lambda \frac{\tau_w}{\mu} \quad , \qquad \tau_w = \mu \frac{\partial u}{\partial n}\Big|_{wall} , \qquad (4)$$

where τ_w is the local wall shear stress. The set of governing equation and the boundary condition form a Poisson equation with slip boundary condition. Because of the geometrical complexities, finding analytical solutions for general cross-section channels are highly unlikely. Therefore, we seek an approximate solution that can predict pressure drop in arbitrary cross-section with reasonable accuracy. This will provide a powerful tool that can be used in many practical instances such as basic design, parametric study, and optimization analyses, where often the trends and a reasonable estimate of the pressure drop is required.

3   CHARACTERISTIC LENGTH SCALE

Selecting an appropriate and consistent characteristics length scale is an important part of developing a comprehensive general model. Selection of the characteristic length is an arbitrary choice and will not affect the final solution. However, a more appropriate length scale leads to more consistent results, especially when general cross-section is considered. A circular duct is fully described with diameter, thus the obvious length scale is the diameter (or radius). For non-circular cross-sections, the selection is not as clear; many textbooks and researchers have conventionally chosen the hydraulic diameter, D_h as the characteristic length. Yovanovich [26, 27] introduced the square root of area ($\sqrt{A}$) as a characteristic length scale for heat conduction and convection problems. Later, Muzychka and Yovanovich [28] proposed the use of $\sqrt{A}$ for the fully-developed flow in non-circular ducts. Bahrami et al. [22, 23] showed through analysis that $\sqrt{A}$ appears in the solution of fully-developed flow in non-circular ducts. They also compared both D_h, $\sqrt{A}$ and observed that using $\sqrt{A}$ as the characteristic length scale results in similar trends in Poiseuille number for microchannels with a wide variety of cross-sections. Therefore, in this study, $\sqrt{A}$ is selected consistently as the length scale throughout the analysis and in the definition of the Knudson number. Using $\sqrt{A}$, Eq. (4) becomes:

$$u_s = \frac{\sigma - 2}{\sigma} Kn \sqrt{A} \frac{\tau_w}{\mu} \qquad (5)$$

4   MODEL DEVELOPMENT

Equation (5) shows that slip-velocity is related to local wall shear stress which depends on the topology of the boundary and the cross-section. Averaging the wall shear stress over the perimeter of the channel, Eq. (5) becomes [29]:

$$\bar{u}_s = \frac{\sigma - 2}{\sigma} Kn \sqrt{A} \frac{\bar{\tau}_w}{\mu} \qquad (6)$$

where $\bar{u}_s$ and $\bar{\tau}_w$ are averaged slip-velocity and wall shear stress, respectively. Using an average (and constant) slip-velocity will simplify the solution to Eq. (3). This allows us to introduce a relative axial velocity, U, which is the difference between the bulk and the slip velocities:

$$U = u - \bar{u}_s \qquad (7)$$

After change of variable Eq. (3) becomes:

$$\frac{dP}{dx} = \mu \left(\frac{\partial^2 U}{\partial y^2} + \frac{\partial^2 U}{\partial z^2} \right) \qquad (8)$$

Based on its definition, the relative velocity is zero on the channel walls. As a result, Eq. (8) becomes the Poisson's

equation with zero boundary condition. It is the same governing equation for fully-developed flow in continuum regime. This equation has been solved for various geometries such as circular, rectangular, and elliptical ducts. The analytical solutions can be found in textbooks such as White [29] and Bejan [30]. A Compact model for determination of Poiseuille number in general cross-section channels have been presented by Bahrami et al. [22, 23].

To determine f Re, Bahrami et al. [22, 23] used the analytical solution of Eq. (8) for elliptical channel. They presented the final result in the following, easy-to-use form:

$$f Re_{\sqrt{A}} = 32\pi^2 I_p^* \frac{\sqrt{A}}{\Gamma} \quad , \qquad I_p^* = \frac{I_p}{A^2} \qquad (9)$$

where I_p^* is the non-dimensional polar moment of inertia of the cross-section. The elliptical channel was considered, not because it is likely to occur in practice, but rather to utilize the unique geometrical property of its velocity solution. The same approach is followed here. Starting from the elliptical cross-section and using the axial relative velocity, one can find the average relative axial velocity $\bar{U}$ for elliptical channels [29]:

$$\bar{U} = \frac{b^2 c^2}{4(b^2 + c^2)} \frac{\Delta P}{\mu L} \qquad (10)$$

Applying a force balance in the channel leads to (see Fig. 1):

$$\bar{\tau}_w \Gamma L = \Delta P \, A \qquad (11)$$

Cross-sectional area and perimeter for elliptical channel are:

$$A = \pi b c$$
$$\Gamma = 4b \, E\left(\sqrt{1 - \varepsilon^2}\right) \qquad (12)$$

where $E(\varepsilon) = \int_0^{\pi/2} \sqrt{1 - \varepsilon x^2} dx$ is the complete elliptic integral of the second kind. Using Eqns. (11) and (12) and defining an aspect ratio, ε, as the ratio of the channel major and minor axes, average velocity can be presented as [22]:

$$\bar{U} = \frac{\sqrt{\varepsilon} E\left(\sqrt{1 - \varepsilon^2}\right)}{\sqrt{\pi^3}(1 - \varepsilon^2)} \frac{\bar{\tau}_w}{\mu} \sqrt{A} \qquad (13)$$

This equation can be rewritten:

$$\bar{U} = \frac{\Gamma \bar{\tau}_w}{16\pi^2 \mu I_p^*} \qquad (14)$$

Using Eqns. (14) and (7), average channel velocity, $\bar{u}$, becomes:

$$\bar{u} = \frac{\Gamma \bar{\tau}_w}{16\pi^2 \mu I_p^*} - \frac{\sigma - 2}{\sigma} Kn \sqrt{A} \frac{\bar{\tau}_w}{\mu} \qquad (15)$$

Introducing Fanning friction factor, $f = 2\bar{\tau}_w / \rho \bar{u}^2$, and after some simplifications, one can write:

$$f Re_{\sqrt{A}} = \frac{2}{\frac{\Gamma}{16\pi^2 \sqrt{A} I_p^*} - \frac{\sigma - 2}{\sigma} Kn}$$
$$, Re_{\sqrt{A}} = \frac{\rho \bar{u} \sqrt{A}}{\mu} \qquad (16)$$

where $Re_{\sqrt{A}}$ is the Reynolds number based on $\sqrt{A}$. Note that Eq. (16) is a general equation; in the continuum limit, where $Kn \to 0$, Eq. (16) yields Bahrami et al. model [22], i.e., Eq. (9). The relationship between f Re for slip-flow regime and the continuum flow is

$$f Re_{\sqrt{A}} = \frac{1}{\frac{1}{f Re_{\sqrt{A}}^{no-slip}} - \frac{\sigma - 2}{2\sigma} Kn} \qquad (17)$$

Following Morini et al. [19], reduction of friction coefficient in slip condition, Φ, can be found

Copyright © ICNMM2008 by ASME

$$\Phi = \frac{fRe_{\sqrt{A}}}{fRe_{\sqrt{A}}^{no-slip}} = \frac{1}{1 + \frac{\sigma - 2}{\sigma}\alpha Kn} \qquad (18)$$

where α was determined through numerical analysis for each geometry by [19]. Using the present model, Eq. (16), Φ can be found from:

$$\Phi = \frac{fRe_{\sqrt{A}}}{fRe_{\sqrt{A}}^{no-slip}} = \frac{1}{1 + \frac{\sigma - 2}{\sigma}\frac{fRe_{\sqrt{A}}^{no-slip}}{2}Kn} \qquad (19)$$

Therefore, Φ can be determined once $fRe_{\sqrt{A}}$ is known for the no-slip condition. Note that the value of Φ is always equal or less than unity.

5   MODEL VERIFICATION

Although the presented approach is based on analytical solution for elliptical cross-section, the final relationship is a function of general geometrical parameters that can be calculated for any cross-sections. In this section, the present model is compared with numerical and experimental data available for several common cross-sections. The proposed model is verified with numerical results of Morini et al. [19] for circular, rectangular, trapezoidal, and double trapezoidal microchannels as well as experimental data published by Kim et al. [4] and Araki et al. [18] for circular and trapezoidal ducts, respectively. For convenience, the geometrical parameters needed for different cross-sections are listed in Table 1. In the following subsections the value of tangential momentum accommodation factor, σ, is assumed to be 1. The available data in the literature were reported based on the hydraulic diameter. The Knudsen and the Poiseuille numbers based on the hydraulic diameter can be converted to $\sqrt{A}$ basis, using the following relationships:

$$fRe_{\sqrt{A}} = fRe_{D_h}\frac{\Gamma}{4\sqrt{A}}$$
$$fRe_{\sqrt{A}} = fRe_{D_h}\frac{\Gamma}{4\sqrt{A}} \qquad (20)$$

5.1   CIRCULAR MICROCHANNELS

Using the geometrical parameters of circular channels listed in Table 1, $fRe_{\sqrt{A}}$ can be determined:

$$fRe_{\sqrt{A}} = \frac{1}{\frac{1}{14.18} - Kn} \qquad , \qquad \sigma = 1 \qquad (21)$$

Morini et al. [19] proposed a similar correlation for $fRe_{\sqrt{A}}$:

$$fRe_{\sqrt{A}} = \frac{fRe_{\sqrt{A}}^{no-slip}}{1 + 8Kn} \qquad (22)$$

In Table 2 the present model is compared with the analytical model proposed by Morini et al. [19], i.e., Eq. (22). As can be seen, the present model yields the exact same values reported by [19] over the slip-flow range of the Knudsen number.

Figure 2 shows the comparison between the present model and experimental data published by Kim et al. [4]. They conducted tests with nitrogen, argon, and helium over a range of $0.0008 < Kn < 0.09$ and $0.03 < Re < 30$. The microtubes used in their experiments were made of quartz glass and had diameters ranging from 5 to 100 micrometers. According to Morini et al. [31] the experimental uncertainty of pressure drop measurements is on the order of 8-14%.

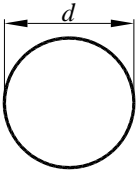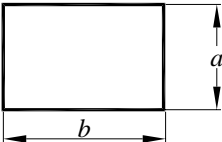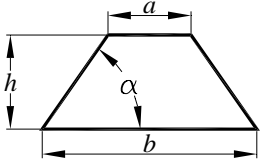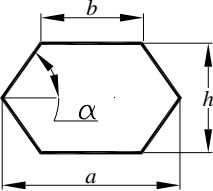**TABLE 1. GEOMETRICAL CHARACTERISTICS OF DIFFERENT CROSS-SECTIONS**

Cross-Section	Area (A)	Perimeter (Γ)	Non-Dimensional Polar Moment of Inertia (I_p^*)	Aspect Ratio
	$\frac{\pi d^2}{4}$	πd	$\frac{1}{2\pi}$	1
	$4bc$	$4(b+c)$	$\frac{1+\varepsilon^2}{12\varepsilon}$	$\frac{b}{c}$
	εh^2	$2h\left(\varepsilon + \sqrt{\varepsilon^2 - \beta\varepsilon^2 + 1}\right)$	$\frac{[2(3\varepsilon^2 + 1) + \beta(-3\varepsilon^2 + 1)]}{36\varepsilon}\varepsilon^2$	$\frac{a+b}{2h}$
	$2\varepsilon h^2$	$4h\left(\sqrt{\varepsilon^2 - \beta\varepsilon^2 + 1}\right)$ $+ 2h\left(\varepsilon - \frac{1}{\tan(\alpha)}\right)$	$\frac{[2(3\varepsilon^2 + 1) + \beta(-3\varepsilon^2 + 1)]}{18\varepsilon}$ $+\frac{8}{9\varepsilon}\left(3 - \frac{1}{\varepsilon \tan(\alpha)}\right)$	$\frac{a+b}{2h}$

Kn	$fRe_{\sqrt{A}}$ (model)	$fRe_{\sqrt{A}}$ [19]	Φ
0	14.180	14.180	1.000
0.001	14.080	14.080	0.993
0.005	13.695	13.695	0.966
0.01	13.241	13.241	0.934
0.03	11.693	11.693	0.825
0.06	9.948	9.948	0.702
0.09	8.656	8.656	0.610
0.1	8.297	8.297	0.585

As can be seen the present model captures the trends of the experimental data over a range of geometrical and thermophysical parameters. Also note that most of data fall within the $\pm10\%$ bounds of the model.

5.2   RECTANGULAR MICROCHANNELS
The geometrical characteristics and schematic of rectangular channels are presented in Table 1. Substituting required parameters in Eq. (16), $fRe_{\sqrt{A}}$ is determined as:

$$fRe_{\sqrt{A}}^{slip} = \frac{1}{\dfrac{1}{\dfrac{4\pi^2(1+\varepsilon^2)}{3\sqrt{\varepsilon}(1+\varepsilon)}} - Kn} \qquad , \sigma = 1 \qquad (23)$$

Table 3 and Fig. 3, show the comparison of the proposed model, Eq. (14) with numerical results of Morini et al. [19] for a range of aspect ratio, $0.01 \le \varepsilon \le 1$. As can be seen, except for a few points, the agreement between the model and the numerical values is less than 8%.

5.3   TRAPEZOIDAL MICROCHANNELS
The cross-section of an isosceles trapezoidal microchannel and its geometrical parameters are presented in Table 1. This is an important shape since this cross-section is formed as a result of etching process in silicon wafers [19]. Furthermore, in the limit when the top side length, a, goes to zero, it yields an isosceles triangle and in another limit when $a=b$, a rectangular channel will be formed. The geometrical characteristics of these limiting cases are listed in Table 4; where β in Tables 1 and 4 is a non-dimensional parameter defined as:

$$\beta = \frac{4ab}{(a+b)^2} \qquad (24)$$

β is zero for triangular and 1 for rectangular conduits. The angle α (as shown in Table 1) is related to β and ε as [22]:

$$sin\,\alpha = \frac{1}{\sqrt{\varepsilon^2 - \beta\varepsilon^2 + 1}} \qquad (25)$$

Bahrami et al. [22] presented the Poiseuille number for the no-slip condition as:

TABLE 3. COMPARISON BETWEEN MODEL AND NUMERICAL DATA [19], RECTANGULAR CROSS-SECTION

$\varepsilon = 0.01$				$\varepsilon = 0.1$				$\varepsilon = 0.3$			
Kn	$fRe_{\sqrt{A}}$ [19]	$fRe_{\sqrt{A}}$ (model)	Error (%)	Kn	$fRe_{\sqrt{A}}$ [19]	$fRe_{\sqrt{A}}$ (model)	Error (%)	Kn	$fRe_{\sqrt{A}}$ [19]	$fRe_{\sqrt{A}}$ (model)	Error (%)
0.0000	119.6	130.3	8.2	0.0000	36.8	38.2	3.6	0.0000	20.8	20.1	3.2
0.0002	118.2	128.6	8.2	0.0006	36.4	37.8	3.6	0.0008	20.6	20.0	3.1
0.0010	112.8	122.4	7.8	0.0029	34.9	36.2	3.7	0.0042	19.8	19.3	2.7
0.0015	109.8	118.8	7.6	0.0043	34.0	35.3	3.7	0.0063	19.4	18.9	2.4
0.0020	106.8	115.4	7.4	0.0057	33.2	34.4	3.7	0.0084	19.0	18.6	2.2
0.0050	92.1	98.5	6.5	0.0144	28.9	30.0	3.7	0.0211	16.8	16.6	1.0
0.0099	74.9	79.2	5.4	0.0287	23.7	24.7	3.7	0.0421	14.1	14.1	0.4
0.0149	63.1	66.2	4.7	0.0431	20.2	20.9	3.7	0.0632	12.1	12.3	1.5
0.0198	54.5	56.9	4.1	0.0575	17.5	18.2	3.8	0.0843	10.7	10.9	2.2
$\varepsilon = 0.6$				$\varepsilon = 0.8$				$\varepsilon = 1$			
Kn	$fRe_{\sqrt{A}}$ [19]	$fRe_{\sqrt{A}}$ (model)	Error (%)	Kn	$fRe_{\sqrt{A}}$ [19]	$fRe_{\sqrt{A}}$ (model)	Error (%)	Kn	$fRe_{\sqrt{A}}$ [19]	$fRe_{\sqrt{A}}$ (model)	Error (%)
0.0000	15.5	14.4	7.1	0.0000	14.5	13.4	7.9	0.0000	14.2	13.2	8.1
0.0010	15.3	14.3	7.0	0.0010	14.4	13.3	7.8	0.0010	14.1	13.1	8.0
0.0048	14.9	14.0	6.5	0.0050	13.9	13.0	7.3	0.0050	13.7	12.7	7.4
0.0073	14.6	13.7	6.2	0.0075	13.7	12.8	7.0	0.0075	13.4	12.5	7.1
0.0097	14.3	13.5	5.9	0.0099	13.4	12.6	6.7	0.0100	13.2	12.3	6.8
0.0242	12.8	12.3	4.3	0.0248	12.1	11.5	5.1	0.0250	11.9	11.3	5.2
0.0484	10.9	10.7	2.3	0.0497	10.4	10.1	3.1	0.0500	10.2	9.9	3.1
0.0726	9.6	9.5	0.8	0.0745	9.1	8.9	1.6	0.0750	8.9	8.8	1.5
0.0968	8.5	8.5	0.3	0.0994	8.1	8.0	0.4	0.1000	8.0	7.9	0.3

$$\text{Error} = \frac{fRe_{\sqrt{A}}\,[19] - fRe_{\sqrt{A}}\,[model]}{fRe_{\sqrt{A}}\,[model]} \times 100$$
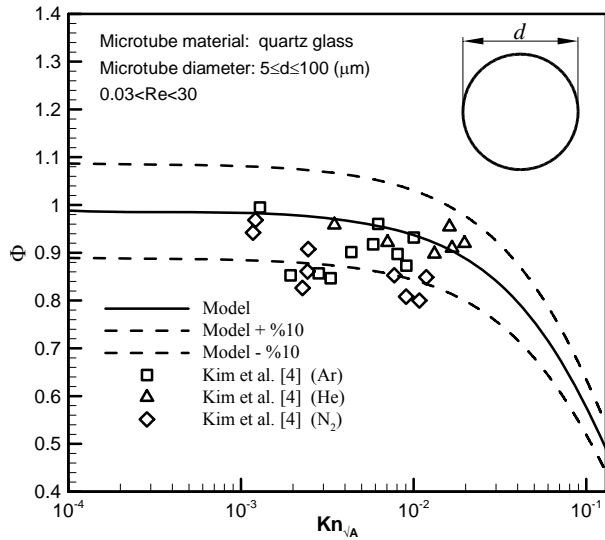
FIGURE 2. COMPARISON OF THE MODEL WITH EXPERIMENTAL DATA OF KIM ET AL. [4] FOR CIRCULAR CHANNELS

$$fRe_{\sqrt{A}}^{no-slip} = \frac{4\pi^2[(3\varepsilon^2+1)+\beta(-3\varepsilon^2+1)]\varepsilon\sqrt{\varepsilon}}{9(\varepsilon+\sqrt{\varepsilon^2-\beta\varepsilon^2+1})} \qquad (26)$$

Using Eqns. (16) and (27) one can calculate $fRe_{\sqrt{A}}$. In Table 5 the predicted results of the proposed model are compared with numerical data of Morini et al. [19] with $\alpha = 54.76°$. The agreement between present model and numerical data is within 8%; however, there are a few points, especially at relatively high or low aspect ratios where differences up to 11% are observed.
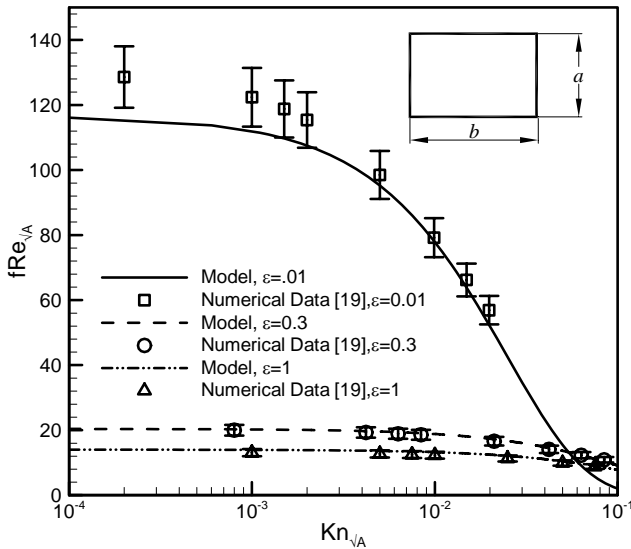

FIGURE 3. COMPARISON OF THE MODEL WITH NUMERICAL RESULTS OF MORINI ET AL. [19] FOR RECTANGULAR CHANNELS

Figure 4 shows the comparison between the proposed model and the experimental data of Araki et al. [18] for trapezoidal microchannels with $\alpha = 54.76°$. They used two different channels with dimensions: $b = 41.5$ and 41.2, $h = 5.56$ and 2.09 micrometers, respectively. These channels were made of silicon wafer with hydraulic diameters of 9.41 and 3.92 micrometers. They conducted tests with nitrogen and helium

over a range of $0.011 < Kn < 0.035$ and $0.05 < Re < 4.2$. The uncertainty of their measurements was reported to be 10.9%.As shown in Fig. 4, the values predicted by the model is within 10% accuracy of the data.
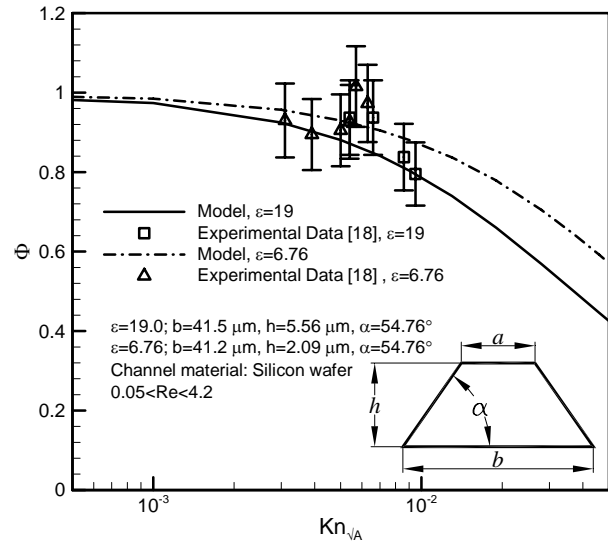

FIGURE 4. COMPARISON OF THE MODEL WITH EXPERIMENTAL DATA OF ARAKI ET AL. [18] FOR TRAPEZOIDAL CHANNELS ($\alpha = 54.76°$)

TABLE 4. LIMITING CASES OF ISOSCELES TRAPEZOID

Cross-section	ε	β	I_p^*	$\sqrt{A}/\Gamma$
Isosceles triangular	$\dfrac{b}{2h}$	0	$\dfrac{3\varepsilon^2+1}{18\varepsilon}$	$\dfrac{\sqrt{\varepsilon}}{2(\sqrt{\varepsilon^2+1}+\varepsilon)}$
Equilateral triangular	$\dfrac{1}{\sqrt{3}}$	0	$\dfrac{\sqrt{3}}{9}$	$\dfrac{\sqrt{3}}{6\sqrt[4]{3}}$
Rectangular	$\dfrac{b}{h}$	1	$\dfrac{\varepsilon^2+1}{12\varepsilon}$	$\dfrac{\sqrt{3}}{2(1+\varepsilon)}$
Square	1	1	$\dfrac{1}{6}$	$\dfrac{1}{4}$

5.4 DOUBLE TRAPEZOIDAL MICROCHANNELS

Double trapezoidal cross-section geometry is depicted in Table1. Same as trapezoidal cross-section, the non-dimensional parameter β is defined by Eq. (24).
Table 6 and Fig. 5 present the comparison between the proposed model with numerical data of Morini et al. [19] for $\alpha = 54.76°$. As can be seen, except for a few points, the agreement between the model and the numerical values is, less than 8%.

6 SUMARRY AND CONCLUSIONS

Pressure drop of fully-developed, incompressible slip-flow through microchannels of general cross-sections is investigated. An averaged first-order Maxwell boundary condition is assumed on the channel walls. Introducing a relative velocity, axial momentum equation reduces to the Poisson's equation with no-slip boundary condition. Following Bahrami et al. [22, 23] and using analytical solution for elliptical microchannels, a compact model is developed that predicts the Poiseuille number as a function of
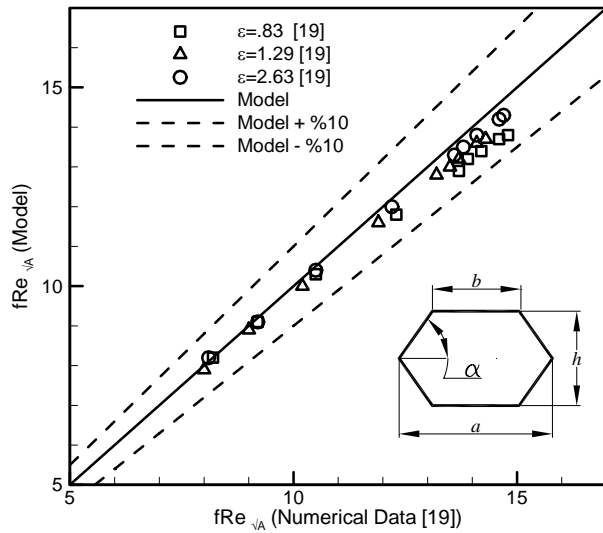
FIGURE 5. COMPARISON OF THE MODEL WITH NUMERICAL DATA OF MORINI ET AL. [19] FOR DOUBLE TRAPEZOIDAL CONDUITS

geometrical parameters of the duct. The presented model is more general than Bahrami et al.'s model and covers both slip-flow and no-slip regimes.

Employing the proposed model, one only needs to compute the non-dimensional parameter $I_p^* A / \Gamma$ of the channel to determine the Poiseuille number. On the other hand, using the conventional method, the Poisson's equation must be solved with slip boundary condition to find the velocity field and the mean velocity often numerically. Then the averaged wall shear stress should be calculated to find f Re. This clearly shows the convenience of the proposed approximate model. The model is successfully validated against existing numerical and experimental data in the literature for a variety of shapes including circular, rectangular, trapezoidal, and double-trapezoidal cross-sections, with a relative difference on the order of 8%.

7 ACKNOWLEDGMENTS

TABLE 5. MODEL VERSUS DATA [19], TRAPEZOIDAL CHANNELS

$\varepsilon = 20.07$				$\varepsilon = 5.07$				$\varepsilon = 2.7$			
Kn	$fRe_{\sqrt{A}}$ [19]	$fRe_{\sqrt{A}}$ (model)	Error (%)	Kn	$fRe_{\sqrt{A}}$ [19]	$fRe_{\sqrt{A}}$ (model)	Error (%)	Kn	$fRe_{\sqrt{A}}$ [19]	$fRe_{\sqrt{A}}$ (model)	Error (%)
0.0000	53.4	56.6	5.6	0.0000	27.1	27.1	0.0	0.0000	18.6	17.9	3.8
0.0004	52.8	56.0	5.6	0.0007	26.8	26.8	0.1	0.0008	18.4	17.8	3.7
0.0021	50.5	53.5	5.5	0.0034	25.7	25.9	0.4	0.0042	17.8	17.3	3.2
0.0031	49.2	52.0	5.4	0.0052	25.1	25.3	0.6	0.0063	17.4	17.0	2.9
0.0041	48.0	50.7	5.4	0.0069	24.6	24.8	0.8	0.0084	17.1	16.7	2.6
0.0104	41.6	43.8	5.0	0.0172	21.6	21.9	1.7	0.0209	15.2	15.1	1.0
0.0207	34.0	35.7	4.7	0.0345	17.9	18.5	2.9	0.0418	12.9	13.0	0.9
0.0311	28.8	30.1	4.4	0.0517	15.3	15.9	3.7	0.0628	11.2	11.5	2.3
0.0415	24.9	26.0	4.2	0.0689	13.4	14.0	4.3	0.0837	9.9	10.2	3.4
$\varepsilon = 1.5$				$\varepsilon = 0.9$				$\varepsilon = 0.8$			
Kn	$fRe_{\sqrt{A}}$ [19]	$fRe_{\sqrt{A}}$ (model)	Error (%)	Kn	$fRe_{\sqrt{A}}$ [19]	$fRe_{\sqrt{A}}$ (model)	Error (%)	Kn	$fRe_{\sqrt{A}}$ [19]	$fRe_{\sqrt{A}}$ (model)	Error (%)
0.0000	15.4	14.5	6.1	0.0000	15.3	13.7	11.5	0.0000	15.4	13.7	12.7
0.0009	15.3	14.4	5.9	0.0009	15.2	13.7	11.3	0.0009	15.3	13.6	12.5
0.0045	14.8	14.0	5.4	0.0045	14.7	13.3	10.6	0.0044	14.8	13.3	11.7
0.0067	14.5	13.8	5.0	0.0067	14.5	13.1	10.1	0.0066	14.5	13.1	11.2
0.0090	14.3	13.6	4.7	0.0089	14.2	12.9	9.7	0.0088	14.3	12.9	10.7
0.0225	12.8	12.5	3.0	0.0223	12.8	11.9	7.4	0.0221	12.8	11.9	8.2
0.0449	11.0	10.9	0.8	0.0447	11.0	10.5	4.5	0.0442	11.0	10.5	4.9
0.0674	9.7	9.7	0.9	0.0670	9.6	9.4	2.2	0.0663	9.6	9.4	2.5
0.0899	8.6	8.8	2.2	0.0894	8.6	8.5	0.5	0.0884	8.6	8.5	0.6

$$\text{Error} = \frac{fRe_{\sqrt{A}}\,[19] - fRe_{\sqrt{A}}\,[model]}{fRe_{\sqrt{A}}\,[model]} \times 100$$

TABLE 6. MODEL VERSUS DATA [19], DOUBLE TRAPEZOIDAL CHANNELS

$\varepsilon = 0.83$				$\varepsilon = 0.96$				$\varepsilon = 1.29$			
Kn	$fRe_{\sqrt{A}}$ [19]	$fRe_{\sqrt{A}}$ (model)	Error (%)	Kn	$fRe_{\sqrt{A}}$ [19]	$fRe_{\sqrt{A}}$ (model)	Error (%)	Kn	$fRe_{\sqrt{A}}$ [19]	$fRe_{\sqrt{A}}$ (model)	Error (%)
0.0000	14.8	13.8	6.6	0.0000	14.7	13.9	6.0	0.0000	14.3	13.7	4.2
0.0010	14.6	13.7	6.5	0.0010	14.6	13.8	5.9	0.0011	14.1	13.6	4.1
0.0050	14.2	13.4	6.1	0.0051	14.1	13.4	5.5	0.0053	13.7	13.2	3.8
0.0075	13.9	13.2	5.8	0.0077	13.9	13.2	5.3	0.0079	13.5	13.0	3.7
0.0100	13.7	12.9	5.5	0.0103	13.6	13.0	5.1	0.0106	13.2	12.8	3.5
0.0251	12.3	11.8	4.2	0.0256	12.3	11.8	4.0	0.0265	11.9	11.6	2.8
0.0501	10.5	10.3	2.5	0.0513	10.5	10.2	2.6	0.0530	10.2	10.0	1.8
0.0752	9.2	9.1	1.2	0.0769	9.2	9.0	1.5	0.0795	9.0	8.9	1.0
0.1002	8.2	8.2	0.2	0.1025	8.2	8.1	0.7	0.1060	8.0	7.9	0.4
$\varepsilon = 1.515$				$\varepsilon = 1.79$				$\varepsilon = 2.63$			
Kn	$fRe_{\sqrt{A}}$ [19]	$fRe_{\sqrt{A}}$ (model)	Error (%)	Kn	$fRe_{\sqrt{A}}$ [19]	$fRe_{\sqrt{A}}$ (model)	Error (%)	Kn	$fRe_{\sqrt{A}}$ [19]	$fRe_{\sqrt{A}}$ (model)	Error (%)
0.0000	14.1	13.6	3.5	0.0000	14.0	13.6	3.0	0.0000	14.7	14.3	2.9
0.0011	14.0	13.5	3.4	0.0011	13.9	13.5	3.0	0.0010	14.6	14.2	2.8
0.0053	13.5	13.1	3.2	0.0054	13.5	13.1	2.8	0.0052	14.1	13.8	2.6
0.0080	13.3	12.9	3.0	0.0080	13.2	12.9	2.6	0.0079	13.8	13.5	2.5
0.0107	13.1	12.7	2.9	0.0107	13.0	12.7	2.5	0.0105	13.6	13.3	2.4
0.0267	11.8	11.5	2.2	0.0268	11.7	11.5	1.9	0.0262	12.2	12.0	1.7
0.0534	10.1	10.0	1.3	0.0536	10.1	10.0	1.0	0.0525	10.5	10.4	0.9
0.0802	8.9	8.8	0.7	0.0803	8.8	8.8	0.4	0.0787	9.2	9.1	0.3
0.1069	7.9	7.9	0.2	0.1071	7.9	7.9	0.1	0.1049	8.1	8.2	0.2

$$\text{Error} = \frac{fRe_{\sqrt{A}}[19] - fRe_{\sqrt{A}}[model]}{fRe_{\sqrt{A}}[model]} \times 100$$

8   REFERENCES

[1] Tuckerman, D. B. and Pease, R. F., 1981, "High-Performance Heat Sinking For VLSI", IEEE Electron Device Letters, Vol. **5**, pp. 126–129.

[2] Hsieh, S.S., Tsai, H. H., Lin, C. Y., Huang, C. F., Chien, C. M., 2004, "Gas Flow in a Long Microchannels," International Journal of Heat and Mass Transfer, Vol. **47**, pp. 3877–3887.

[3] Zhu, X., Lao, Q., and Xin, M. D., 2006, "Gas Flow in Microchannel of Arbitrary Shape in Slip Flow Regime," Journal Thermophysical Heat Transfer, Vol. **18** (1), pp. 65–72.

[4] Kim, M. S., Araki, T., Inaoka, K., Suzuki, K., 2000, "Gas Flow Characteristics in Microtubes," JSME International Journal, Vol. **43** (4), pp. 634-639.

[5] Bahrami, M., Yovanovich, M. M., and Culham, J. R., 2006, "Pressure Drop of Fully-Developed, Laminar Flow in Rough Microtubes," ASME Journal of Fluids Engineering, Vol. **128**, pp. 632–637.

[6] Morini, G. L., 2004, "Laminar-To-Turbulent Flow Transition in Microchannels," Microscale Thermophysical Engineering, Vol. **8**, pp. 15–30.

[7] Wu, H. Y. and Cheng, P., 2003, "Friction Factors in Smooth Trapezoidal Silicon Microchannels with Different Aspect Ratios," International Journal of Heat and Mass Transfer, Vol. **46**, pp. 2519-2525.

[8] Renksizbulut, M., Niazmand, H., and Tercan, G. 2006, "Slip Flow and Heat Transfer in Rectangular Microchannels with Constant Wall Temperature," International Journal of Thermal Science, Vol. **45**, pp. 870–881.

[9] Pfahler, J., Harley, J., Bau, H., and Zemel, J.N., 1991, "Gas and Liquid Transport in Small Channels," ASME Micromech. Sensors Actuators Systems, Vol. **32**, 49-58.

[10] Ebert, W.A. and Sparrow, E.M., 1965, "Slip Flow in Rectangular and Annular Ducts," ASME Journal of Basic Engineering, Vol. **87**, pp. 1018-1024.

[11] Harley, J., Huang, Y., Bau, H., and N. Zemel, J., 1995, "Gas Flow in Microchannels," Journal of Fluid Mechanics, Vol. **284**, pp. 257–274.

[12] Morini, G.L. and Spiga, M., 1998, "Slip Flow in Rectangular Microtubes," Microscale Thermophysical Engineering, Vol. **2**(4), pp. 273-282.

[13] Beskok, A. and Karniadakis, G. E., 1999, "A Model for Flows in Channels, Pipes, and Ducts at Micro Scales," Microscale Thermophysical Engineering, Vol. **3**, pp. 43-77.

[14] Yu, d., Warrington, R., Barron, R., and Ameel, T., 1995, "Fluid Flow and Heat Transfer in Microtubes," ASME/JSME, Thermal Engineering Conference, Vol. **1**, pp. 523-530.

[15] Choi, S. B., Barron, R. F. and Warrington, R. O., 1991, "Fluid Flow and Heat Transfer in Microtubes", ASME, Micromechanical Sensors, Actuators, and Systems, Vol. **32**, pp. 123-134.

[16] Arkilic, E. B., Schmidt, M. A., and Breuer, K. S., 1997,

"Gaseous Slip Flow in Long Micro/Nano-Channels, Journal of Microelectromechanical Systems," Vol. **6**(2), pp. 167-178.

[17] Arkilic, E. B., Breuer, K. S., and Schmidt, M. A., 2001, "Mass Flow and Tangential Momentum Accommodation in Silicon Micromachined Channels," Journal of Fluid Mechanics, Vol. **43** (7), pp. 29-43.

[18] Araki, T., Kim, M. S., Hiroshi, I., Suzuki, K., 2000, "An Experimental Investigation of Gaseous Flow Characteristics in Microchannels," Proceedings of international conference on heat transfer and transport phenomena in microscale. Begell House, New York, pp. 155–161.

[19] Morini, G.L., Spiga and M., Tartarini, P., 2004, "The Rarefaction Effect on the Friction Factor of Gas Flow in Micro/Nano-Channels," Superlattices and Microstructures, Vol. **35**(3), pp. 587-599.

[20] Khan, W. A. and Yovanovich, M. M., 2007, "Analytical Modeling of Fluid Flow and Heat Transfer in Micro/Nano-Channel Heat Sinks", Proceedings of IPACK2007, Vancouver, British Columbia, Canada.

[21] Duan, Z. and Muzychka, Y. S., 2007, "Slip Flow in Non-Circular Microchannels" Microfluid Nanofluid, Vol. **3**, pp. 473-484.

[22] Bahrami, M., Yovanovich, M. M., and Culham, J. R., 2006, "Pressure Drop of Laminar, Fully Developed Flow in Microchannels of Arbitrary Cross-Section", ASME J. of Fluid Engineering, Vol. **126**, pp. 1036-1044.

[23] Bahrami, M., Yovanovich, M. M. and Culham, J. R., 2007, "A Novel Solution for Pressure Drop in Singly Connected Microchannels," Int. J. of Heat and Mass Transfer, Vol. **50**, pp. 2492-2502.

[24] Roy, S. and Raju, R., 2003, "Modeling gas Flow through Microchannels and Nanopores," Journal of Applied Physics, Vol. **93**, pp. 4870-4879.

[25] Karniadakis, G. E. and Beskok, A., 2002, "Micro flows, fundamentals & simulation", Springer Verlag, New York.

[26] Yovanovich, M.M., 1974, "A General Expression for Predicting Conduction Shape Factors," AIAA, Thermophysics and Space Craft Control, Vol. **35**, pp. 265-291.

[27] Yovanovich, M.M., 1987, "New Nusselt and Sherwood Numbers for Arbitrary Isopotential Bodies at Near Zero Peclet and Rayleigh Numbers," AIAA 22nd Thermophysics Conf., Honolulu, Hawaii.

[28] Muzychka, Y.S. and Yovanovich, M.M., 2002, "Laminar flow friction and heat transfer in non-circular ducts and channels part 1: Hydrodynamic problem," Compact Heat Exchangers, A Festschrift on the 60th Birthday of Ramesh K. Shah, Grenoble, France, pp. 123–130.

[29] White, F. M., 1984, "Viscous Fluid Flow", McGraw-Hill, New York.

[30] Bejan, A. 1995, "Convection Heat Transfer", John Wiley and Sons, New Jersey.

[31] Morini, G. L., Lorenzini, M. and Spiga M., 2005, "A Criterion for Ecperimental Validation of Slip-Flow Models for Incompressible Rarefied Gases through Microchannels," Microfluid Nanofluid, Vol. **1**, pp. 190-196.